Value of ^{18}F-FET PET in Patients With Suspected Tumefactive Demyelinating Disease—Preliminary Experience From a Retrospective Analysis

Massimo Barbagallo, Abdulrahman A. Albatly, MD,*† Simon Schreiner, MD,‡ Helen K. Hayward-Könnecke, MD,‡ Alfred Buck, MD,* Spyros S. Kollias, MD,§ and Martin W. Huellner, MD**

Purpose: To investigate the diagnostic value of ^{18}F-fluoroethyl-*L*-tyrosine (FET) positron emission tomography (PET) in patients with suspected tumefactive demyelinating disease.

Methods: We retrospectively examined FET-PET and MR imaging of 21 patients (12 female, 9 male) with known demyelinating disease and newly diagnosed tumefactive lesions. The maximum standardized uptake value (SUV_{max}), time activity curves (TAC) and lesion-to-background ratio (TBR) of these lesions were calculated. The standard of reference consisted of biopsy and/or follow-up imaging. FET parameters of true neoplastic lesions and tumefactive demyelinating lesions were compared using Mann-Whitney U-test and receiver operating characteristic (ROC) analysis.

Results: Nine patients (42.9%) had neoplastic lesions, 12 patients (57.1%) had tumefactive demyelinating lesions. TBR_{max}, SUV_{max} and TAC were significantly different between demyelinating lesions and neoplastic lesions: Tumors had a higher TBR_{max} (3.53 ± 1.09 vs. 1.48 ± 0.31, respectively; $P < 0.001$) and SUV_{max} (3.95 ± 1.59 vs. 1.86 ± 0.50, respectively; $P < 0.001$) than tumefactive demyelinating lesions. The TAC of tumors was significantly higher compared to tumefactive demyelinating lesions at all time points ($P < 0.05$). ROC analysis revealed that a TBR_{max} threshold of 2.2 and a SUV_{max} threshold of 2.5 could reliably differentiate tumor and tumefactive demyelination (area under the curve, 1.000 and 0.958, respectively).

Conclusion: In patients with demyelinating disease, FET-PET parameters TBR_{max} (cut-off 2.2) and SUV_{max} (cut-off 2.5) are able to distinguish tumefactive demyelinations from true neoplastic lesions.

Key Words: demyelinating disease, multiple sclerosis, ADEM, Balo, 18F-FET, PET, tyrosine, PET/CT, brain tumors, glioblastoma, central lymphoma, MR, PET/MR

(*Clin Nucl Med* 2018;43: e385–e391)

Several types of inflammatory demyelinating diseases (IDD) may exhibit tumefactive characteristics, such as the comparatively rare "classic" tumefactive multiple sclerosis (TMS), acute disseminated encephalomyelitis (ADEM, a multifocal demyelinating disease often seen after an infectious illness), Balo's concentric disease, as well as pattern III multiple sclerosis.[1,2] Patients with single tumefactive demyelinating lesions (TDL), being considered a separate entity on a spectrum between MS and ADEM, occasionally proceed to multiple sclerosis.[1,3–6] For the purpose of our study, the term tumefactive demyelinating disease (TDD) is used as umbrella term for all of the aforementioned entities.

TMS is defined as a large (>2 cm) lesion on radiologic imaging, which is often accompanied by edema and mass effect and shows ring enhancement.[1,7,8] However, a recent trial showed that lesions <2 cm may exhibit similar imaging characteristics, reflecting the ambiguity of the definition of TMS lesions.[8] So far, no large-scale epidemiological data is available on TDD.[1,7] In older trials, the incidence of TDD was estimated 0.3 cases per 100,000 population per year, and the prevalence 1–2 per 1000 cases of MS,[9–11] with a slight female predominance. The mean age at TDD onset is between 30 and 40 years. The incidence of ADEM varies between 0.07 and 0.64 per 100,000 per year. Specific epidemiological data on Balo's concentric disease is lacking.[12–14]

Clinical symptoms of TDD depend on lesion size, location and mass effect. Lesions are typically found in the white matter of the frontal and parietal lobes as well as in the corpus callosum.[1,6,7] Similar to tumors, TDD may appear as solitary lesion or multiple lesions, and might exhibit signal characteristics on magnetic resonance (MR) imaging similar to neoplastic brain lesions.[1,9,15] Not only its presentation on diagnostic imaging, but also the clinical presentation of TDD might mimic a neoplastic brain lesion, including the event of acute life-threatening situations.

In order to achieve a definite diagnosis, stereotactic biopsy with subsequent histopathological examination is considered standard of reference. Although severe complications of stereotactic biopsy, such as major bleeding or infection, are rather uncommon, the invasive nature of the procedure still exposes the patient to a certain risk, and is comparably expensive.[1]

Cases of TDD and synchronous or metachronous brain tumors have been reported.[16–18] Several studies suggested an association between MS and astrocytoma, oligodendroglioma and glioblastoma.[19–21] However, such possible associations might be misleading. It is not known if the possible higher rate of neoplastic brain lesions in MS patients is purely incidental due to frequent follow-up neuroimaging scans (surveillance bias), or if causative factors are present in patients with demyelinating disease. Such might be the inflammation in the context of disease itself or its treatment with immunomodulating drugs, which might promote the development of brain tumors.[22] Moreover, it is not well understood if demyelinating lesions and glial tumors—if associated—have a different course.[22]

Positron emission tomography (PET) imaging using the radiotracer ^{18}F-fluoroethyl-*L*-tyrosine (FET) was shown useful in brain lesions, e.g. for the discrimination of low-grade tumors

Received for publication May 14, 2018; revision accepted July 5, 2018.
From the *Department of Nuclear Medicine, University Hospital Zurich/University of Zurich, Rämistrasse, Zürich, Switzerland; †Department of Diagnostic Radiology, Prince Sultan Medical Military City, Riyadh, Saudi Arabia; ‡Neurology Clinic, University Hospital Zurich/University of Zurich, Frauenklinikstrasse; and §Department of Neuroradiology, University Hospital Zurich/University of Zurich, Rämistrasse, Zürich, Switzerland.
Conflicts of interest and sources of funding: M.W.H. received speaker's fees from GE Healthcare. The institution of M.B., M.W.H., A.A.A., and A.B. received grants from GE Healthcare. None declared to all other authors.
Correspondence to: Martin W. Huellner, MD, Department of Nuclear Medicine, University Hospital Zurich/University of Zurich, Rämistrasse 100, 8091 Zürich, Switzerland. E-mail: martin.huellner@usz.ch.

ISSN: 0363-9762/18/4311–e385
DOI: 10.1097/RLU.0000000000002244

and non-neoplastic lesions from high-grade tumors and lymphoma.[23–26] FET is taken up selectively into tumor tissue, and accumulates rather slowly in non-tumoral tissue.[27–30] FET-PET as non-invasive tool was also shown useful for biopsy guidance, as well as treatment planning and monitoring.[31–34]

To date, the available literature on the diagnostic value of FET-PET in patients with suspected TDD is limited to a single case report, which showed a benefit of FET-PET for the differentiation of tumefactive demyelination from neoplastic brain lesions.[17] Thus, the aim of our study was to investigate the diagnostic value of FET-PET in patients with suspected TDD, particularly for the discrimination of tumefactive demyelinations from true brain tumors.

MATERIALS AND METHODS

This retrospective study was accepted by the local ethics committee. Our institution uses a general consent form for all retrospective studies since 2014. Only patients who signed this consent form were included. Informed consent was waived for patients scanned before 2014. Patients with documented refusal of consent to retrospective studies were not enrolled into our study. The radiotracer FET-PET is approved for the work-up of suspected brain tumors in our country.

Clinical Data

Our hospital serves as a national reference center for the diagnosis and treatment of brain tumors.

Patients fulfilling the following criteria were included into our study: diagnosis of demyelinating disease; newly diagnosed tumefactive lesion; available MR scan with T1-weighted (T1w) post-contrast images, fluid-attenuated inversion recovery (FLAIR)-weighted images and diffusion-weighted images (DWI); FET-PET scan performed for further characterization of the lesion. As a matter of fact, this limits our study cohort to patients with equivocal or inconclusive MR scans. A query in the radiological information system, using the keywords "multiple sclerosis," "MS," "demyelinating" and "tumefactive" in conjunction with the imaging modality FET-PET, yielded 25 patients. Of those, four patients were subsequently not included due to refusal of consent. Clinical and demographic data are given in Table 1.

TABLE 1. Demographic Data of Patients

Age	
Median ± SD (y)	47.0 ± 14.9
Range (y)	21–72
Gender	
Female (n (%))	12 (57.1)
Male (n (%))	9 (42.9)
Previously diagnosed demyelinating disease	
Primary progressive MS (n (%))	3 (14.3)
Relapsing-remitting MS (n (%))	7 (33.3)
TMS (n (%))	2 (9.5)
Clinically isolated syndrome (n (%))	5 (23.8)
Balo concentric sclerosis	1 (4.8)
ADEM (n (%))	3 (14.3)
Reason for referral: suspicion of…	
ADEM or brain tumor (n (%))	3 (14.3)
Balo or brain tumor (n (%))	1 (4.8)
TMS or brain tumor (n (%))	2 (9.5)
PML or brain tumor (n (%))	7 (33.3)
Tumefactive demyelination or brain tumor (n (%))	8 (38.1)
Therapy at time of scan	
Natalizumab (n (%))	6 (28.6)
Steroids (n (%))	6 (28.6)
Glatiramer acetate (n (%))	2 (9.5)
No therapy (n (%))	5 (23.8)
Fingolimod (n (%))	1 (4.8)
Fingolimod + steroids (n (%))	1 (4.8)
Interferon β-1a followed by dimethyl fumarate (n (%))	1 (4.8)

ADEM indicates acute disseminated encephalomyelitis; MS, multiple sclerosis; PML, progressive multifocal leukoencephalopathy; SD, standard deviation; TMS, tumefactive multiple sclerosis.

Image Analysis

Imaging analysis included the FET-PET scan mentioned above, and the last MR scan before the FET-PET scan.

MR Imaging

The size and volume of the tumefactive lesion was assessed on FLAIR-weighted images. The borders of the lesion were characterized on FLAIR-weighted images as well-defined or ill-defined. Other observed features concerned the presence of contrast enhancement on T1w images, the presence of perilesional edema on T2-weighted (T2w) images, presence of signs of cerebrospinal fluid (CSF) circulation impairment, presence of restricted diffusion on DWI and apparent diffusion coefficient (ADC) map. The ADC signal was subdivided into bright, mixed or dark appearance. Finally, the time distance between MR exam and FET-PET scan was recorded. Owing to the retrospective nature of our study, MR exams were carried out on different MR scanners.

FET-PET Imaging

FET-PET exams were carried out on Discovery VCT scanner (GE Healthcare, Waukesha WI) or a Discovery 690 Standard scanner (GE Healthcare). The standard protocol used at our institution requires an injection of 130 MBq of ^{18}F-FET. The dynamic FET-PET acquisition started 20 min after tracer injection, using four 5 min frames, with a total acquisition time of 20 min. Dynamic and static PET image datasets were reconstructed from raw data. Emission data was corrected following a standardized procedure (randoms, dead time, scatter, attenuation). The attenuation-corrected axial PET datasets were reconstructed assuming a matrix size of 128 × 128 pixels (voxel spacing: 2.3438 × 2.3438 × 3.27). All FET-PET data analyses were conducted using PMOD® 3.7 (PMOD technologies, Zürich, Switzerland), which allows for a retrospective co-registration of FET-PET and MR images.

The following FET-PET parameters were assessed: the maximum standardized uptake value (SUV_{max}), tumefactive lesion-to-background ratio (TBR_{max}) and time activity curve (TAC) pattern. TBR_{max} was derived by dividing the SUV_{max} of the lesion by the SUV_{mean} of the contralateral normal parietal lobe. As suggested by Calcagni et al., the slope of the TAC was subdivided into three different types.[24] The first type (so-called "wash-in") shows an increase of more than 10% during dynamic acquisition. The second type ("plateau") shows a stable curve with less than 10% change over time. The third type ("wash-out") shows a decrease of more than 10%. According to Pöpperl et al., the sum of the frame-to-frame differences (SoD) in SUV_{max} was calculated using the formula $\Sigma\,(n_i - n_{i-1})$.[25]

Standard of Reference

All available surgery and/or biopsy results were considered. If histopathology was not available, clinical and imaging follow-up was considered. Shrinkage of lesions over time in the

TABLE 2. Final Diagnosis of Lesions

Standard of reference	
Histopathology (stereotactic biopsy) (n (%))	6 (28.6)
Histopathology (surgical biopsy) (n (%))	7 (33.3)
Clinical and imaging follow-up (n (%))	8 (38.1)
Final diagnosis	
Demyelination (n (%))	12 (57.1)
Neoplastic tumor (n (%))	9 (42.9)
Tumor type	
Glioblastoma (n (%))	5 (23.8)
Lymphoma (n (%))	2 (9.5)
Oligodendroglioma (n (%))	1 (4.8)
Gliomatosis cerebri (n (%))	1 (4.8)
Tumor grade according to WHO	
IV (n (%))	5 (23.8)
III (n (%))	2 (9.5)

Although listed in the WHO classification system and being considered high-grade lesions, cerebral lymphomas are primarily characterized by their cell of origin and are not assigned to a specific grade.

WHO indicates World Health Organization.

absence of tumor-specific therapy was defined to indicate a non-neoplastic nature of the lesion.

Statistical Analysis

Ordinal and non-dichotomous variables are presented as median with ranges. Nominal variables and non-dichotomous variables are presented as mode (in percentage), while ratio variables are presented as geometric mean with added/subtracted standard deviation. FET-PET parameters of true neoplastic lesions and tumefactive demyelinating lesions were compared using Mann-Whitney U-test. According to the standard of reference, the area under the ROC curve and the 95% confidence intervals were calculated, fitted for SUVmax and TBRmax. *P*-values of less than 0.05 were considered to indicate significance. All statistical analysis were carried out using SPSS® version 22 (IBM, Armonk, NY).

TABLE 3. MR Characteristics of Lesions

	Neoplastic Tumors (n = 9)	Tumefactive Demyelinations (n = 12)
Volume on FLAIR		
Mean ± SD (cm^3)	17.4 ± 15.0	11.0 ± 13.1
Contrast enhancement		
Yes (n (%))	6 (66.7)	10 (83.3)
No (n (%))	3 (33.3)	2 (16.7)
FLAIR borders		
Well-defined (n (%))	4 (44.4)	4 (33.3)
Ill-defined (n (%))	5 (55.6)	8 (66.7)
Presence of diffusion restriction		
Yes (n (%))	4 (44.4)	5 (41.7)
No (n (%))	5 (55.6)	7 (58.3)
Presence of perilesional edema		
Yes (n (%))	5 (55.6)	6 (50.0)
No (n (%))	4 (44.4)	6 (50.0)
ADC signal		
Bright (n (%))	3 (33.3)	7 (58.3)
Mixed (n (%))	4 (44.4)	5 (41.7)
Dark (n (%))	2 (22.2)	0 (0.0)

ADC indicates apparent diffusion coefficient; FLAIR, fluid-attenuated inversion recovery; SD, standard deviation.

RESULTS

Between January 2001 and December 2016, 21 patients were included. Demographic data including reason for referral are summarized in Table 1. The median interval between MR scan and FET-PET scan was 13 ± 45.0 days. The most common location of the culprit lesion was the supratentorial deep white matter (6/21 patients, 28.6%), followed by the white matter of the frontal lobes (5/21 patients, 23.8%) and temporal lobes (5/21 patients, 23.8%). The remainder of lesions was located in the white matter of the parietal lobe, in the thalamus and in the infratentorial area.

Final diagnosis of lesions is given in Table 2. Nine patients (42.9%) had true neoplastic lesions and 12 patients (57.1%) had non-neoplastic tumefactive demyelinating lesions. Eleven patients (52.3%) with previously diagnosed multiple sclerosis were under MS-specific therapy. Seven thereof underwent biopsy, and histopathology revealed tumefactive demyelinations in four patients, and neoplastic tumors in the other three patients (glioblastoma, lymphoma). The age of patients with true neoplastic lesions and non-neoplastic tumefactive demyelinating lesions was not different (51.4 ± 10.0 years vs. 45.6 ± 17.7 years, respectively; $P = 0.337$).

MR imaging features of lesions are given in Table 3. The size of tumors and TDL was comparable ($P = 0.102$). CSF circulation impairment occurred in one patient with gliomatosis cerebri.

For the FET-PET scans, patients were injected with an average dose of 131.9 ± 4.6 MBq. FET-PET parameters of brain tumors and TDL are given in Table 4. SUV_{max} and TBR_{max} were significantly higher in brain tumors than in TDL. Tumors had a higher TBR_{max} (3.53 ± 1.09 vs. 1.48 ± 0.31, respectively; $P < 0.001$) and SUV_{max} (3.95 ± 1.59 vs. 1.86 ± 0.50, respectively; $P < 0.001$) than tumefactive demyelinating lesions.

The dynamic FET uptake of TDL and neoplastic lesions is shown in Figure 1. The receiver operating characteristic (ROC) analysis revealed that a TBR_{max} threshold of 2.2 and a SUV_{max} threshold of 2.5 are able to reliably differentiate tumors and tumefactive demyelinations (area under the curve, 1.000 (confidence interval, 1.000–1.000) and 0.958 (confidence interval, 0.000–1.000), respectively). Figure 2 shows the distribution of TBR_{max} in TDL and

TABLE 4. FET-PET Data of Lesions

	Neoplastic Tumors (n = 9)	Tumefactive Demyelinations (n = 12)
SUV_{max}		
Mean ± SD	3.95 ± 1.59	1.86 ± 0.50
TBR_{max}		
Mean ± SD	3.53 ± 1.09	1.48 ± 0.31
Curve pattern		
Wash-in (n (%))	1 (11.1)	7 (58.3)
Plateau (n (%))	0 (0.0)	4 (33.3)
Wash-in, then wash-out (n (%))	8 (88.9)	1 (8.3)
Sum of differences		
Mean ± SD	−0.08 ± 0.36	0.21 ± 0.16

SD indicates standard deviation; SUV_{max}, maximum standardized uptake value; TBR_{max}, maximum tumefactive lesion-to-brain ratio.

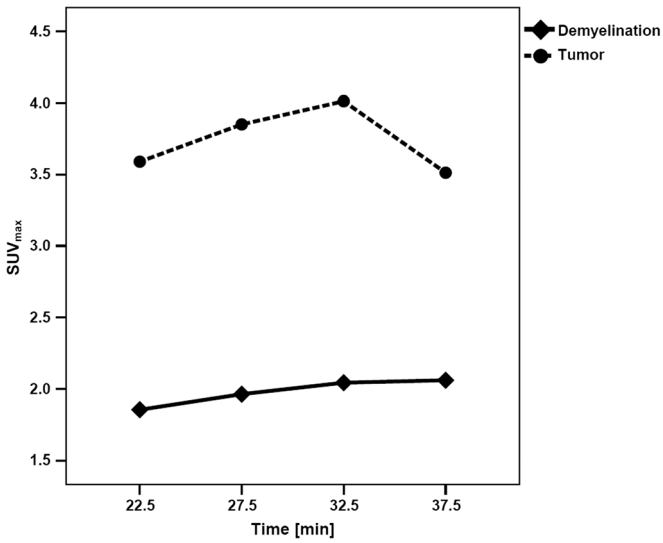

FIGURE 1. Dynamic ^{18}F-FET uptake of lesions. The graph shows the maximum standardized uptake value (SUV_{max}) of tumefactive demyelinations and neoplastic tumors. Mann-Whitney U-test revealed significant differences at all time points (22.5 min, $P = 0.004$, 27.5 min, $P = 0.004$, 32.5 min, $P = 0.001$, 37.5 min, $P = 0.006$).

neoplastic lesions. Values ranged from 1.0–1.9 in TDL and 2.4–5.5 in tumor lesions.

DISCUSSION

Because the discrimination of tumefactive demyelinating lesions and neoplastic lesions with MR is oftentimes challenging, and misinterpretation might possibly have severe consequences, the aim of our study was to investigate the use of non-invasive FET-PET for this purpose. FET-PET scans are an established tool for detection, observation and differentiation of supratentorial brain tumors and for the estimation of prognosis in patients with gliomas.[23–25,31,35] Potential diagnostic benefits of FET-PET scans for the differentiation of neoplastic lesions and TDL have yet not been investigated systematically. Up to now, the only evidence indicating a potential benefit of this imaging method is one single case report.[17]

In our study, we observed significantly higher TBR_{max} and SUV_{max} in brain tumors compared to TDL. As shown in Figure 2, no overlap of TBR_{max} in TDL and neoplastic lesions was observed, rendering this parameter highly accurate. ROC analysis revealed an optimal cut-off at a TBR_{max} of 2.2. These findings are consistent with findings by Rapp et al. who established a similar threshold for discriminating low-grade tumors and high-grade tumors.[23] In our cohort, there were no low-grade tumors, which is likely due to the inclusion criteria. Apparently, high-grade tumors are more likely to meet the clinical presentation and radiological criteria of TDL than low-grade tumors, owing to their comparably fast growth and invasive behavior. Typical MR features of high-grade tumors are e.g. contrast enhancement and presence of cystic/necrotic areas. The spread of TBR_{max} values of TDL was smaller compared to neoplastic lesions, probably reflecting a larger metabolic heterogeneity among different types of tumors. Neoplasms in our cohort consisted of glioblastoma, oligodendroglioma, gliomatosis cerebri as well as lymphoma.

The SUV_{max} of high-grade brain tumors in our cohort are comparable with the literature.[24] Also this parameter yielded a high discriminatory power in the ROC analysis, with an optimal cut-off obtained at 2.5. As shown by previous studies, late TAC kinetics (20–40 min) are important for the discrimination of high-grade tumors and inflammatory lesions.[24,36] Since our study was conducted retrospectively in patients who underwent a clinical PET with limited acquisition time, data on the time to peak of the TAC cannot be derived for every lesion, and is therefore not discussed. Our TAC analysis shows that the SUV_{max} was significantly different in tumors and demyelinating lesions at every PET frame. In accordance with pertinent literature, the typical TAC pattern in neoplastic lesions in our cohort was a wash-in, followed by a wash-out, which was found in 89%.[24,25] For TDL, we could not detect a specific TAC pattern. Only one single TDL displayed the aforementioned wash-out pattern, which is frequently observed in high-grade neoplastic lesions. Hence, presence of a wash-out pattern might be useful for the differentiation of (high-grade) tumors and TDL using dynamic FET-PET. The exact mechanisms of FET wash-out in high-grade brain tumors are not completely understood, but probably rely on a combination of passive efflux and active transport. Notably, our study does not provide information on the differentiation of TDL from *low-grade* tumors.

Histopathological examination is the accepted standard of reference to distinguish neoplastic lesions and TDL, but is not always practicable, owing to invasiveness, potential complications and limitations due to the anatomical location of lesions. Furthermore, misinterpretation of TDL as neoplastic lesions due to a hypercellular pattern, atypical reactive astrocytosis and mitotic figures are possible.[37,38] In the trial of Lucchinetti et al., misdiagnosis occured in approximately 30% of biopsies.[1]

Although TDL might be an overall rare finding in MR scans of patients with demyelinating disease, a reliable differentiation from true neoplastic lesions is important in order to allow for appropriate therapy. As shown in Figure 3 and Figure 4, MR characteristics of tumefactive demyelinations and neoplastic lesions may appear similar and are oftentimes not specific for either entity. Several contrast enhancement patterns have been described for TDL, such as homogenous, heterogeneous, nodular, or closed vs. open rings pointing towards gray matter.[1,9,39] In our cohort, presence or absence of MR contrast enhancement and/or perilesional edema could not distinguish TDL from neoplastic lesions. This is not only

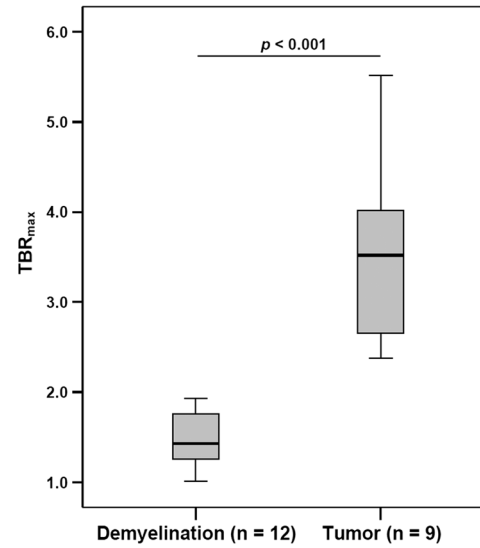

FIGURE 2. Boxplot of TBR_{max} of tumefactive demyelinations and neoplastic tumors. The horizontal borders correspond to the median and the 25th and 75th percentile, respectively. Whiskers indicate the minimal and maximal value.

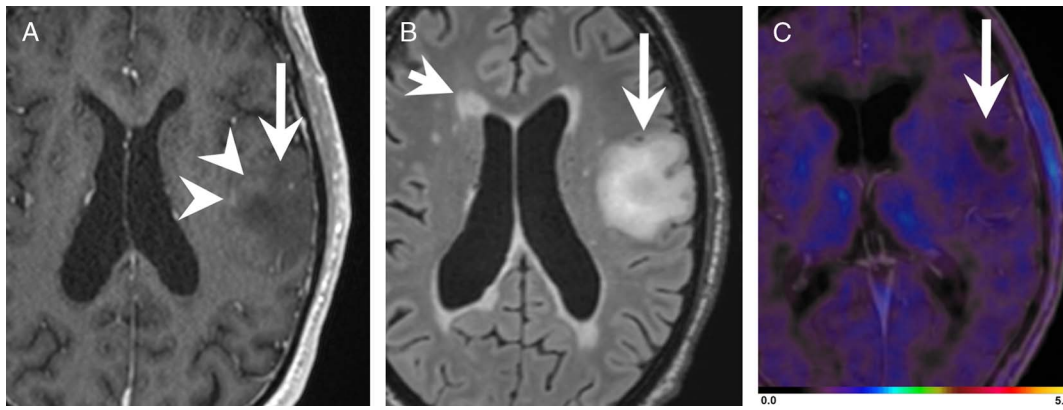

FIGURE 3. Tumefactive demyelinating lesion in a patient with demyelinating disease. The new appearing lesion in the left-sided frontal lobe (arrow) shows patchy contrast enhancement (arrowheads) at the rim on the T1-weighted MR image (**A**). The lesion (arrow) is hyperintense on the FLAIR-weighted MR image (**B**). Other demyelinations are seen throughout the brain, e.g. in subependymal location adjacent to the right-sided frontal horn (short arrow). FET-PET (**C**) co-registered with the T1-weighted MR image reveals very low uptake of the lesion (arrow, SUV_{max} 1.9, TBR_{max} 1.2), with a completely FET-negative center.

a result of our selection criteria, which basically revert to MR scans being equivocal for the discrimination of both entities, but these findings are also reflected by the currently ambiguous definition of TMS lesions. FLAIR borders and volume of lesions were also not helpful for differentiating demyelinating lesions and neoplastic lesions in our cohort. However, as described by Floeth et al., lesion borders on FLAIR-weighted images might still harbor prognostic value for low-grade gliomas.[31] Fliss et al. showed in a hybrid PET/MR study, that FET-PET and perfusion-weighted MR in fact yield different information in patients with brain tumors, with larger tumor volumes obtained with FET-PET than with the regional cerebral blood volume derived from MR.[33] However, their study did not contain demyelinating lesions, and our study does not contain perfusion MR imaging. Hence, possible conclusions are limited. Nevertheless, multimodal hybrid imaging, such as PET/MR, might provide diagnostic benefits compared to sequential single modality imaging in patients with neoplastic lesions, since the correlation with histopathological malignancy indices is probably more consistent.[40]

Also the ADC signal could not discriminate demyelinating lesions and neoplastic lesions in our cohort. In our cohort and corresponding to pertinent literature, TDL are consistently of bright or intermediate signal intensity on ADC, but not dark. This might be related to the presence of vasogenic edema. MS lesions are also well known to change their ADC signal during disease progression.[41–43] Overall, there was a significant overlap of the ADC signal of TDL and true neoplastic lesions in our cohort.

Altogether, our results show that TDL might be distinguished from brain tumors using FET-PET, if conventional MR imaging is not able to answer this question.[3,44] Both the misinterpretation of a neoplastic lesion as demyelinating disease and vice versa might expose the patient to unnecessary risks, be it delayed surgery or chemoradiation treatment in the first case, or unnecessary treatment in the latter one.[45] Also an initial high-dose steroid therapy, which is occasionally given to reduce the perilesional edema in neoplastic lesions as well as for immunosuppression in MS patients, may eventually lead to an exacerbation of neoplastic lesions.[46,47]

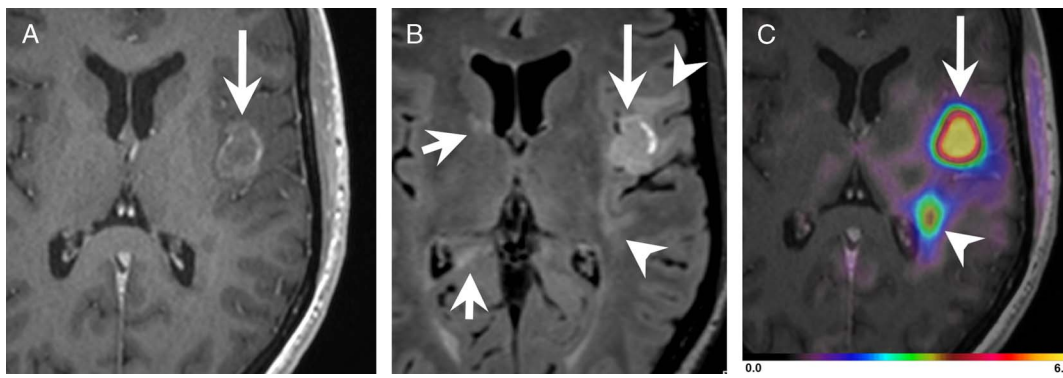

FIGURE 4. Glioblastoma multiforme in an MS patient. The new appearing lesion in the left-sided insula (arrow) shows some contrast enhancement, predominantly at the rim on the T1-weighted MR image (**A**). The lesion (arrow) is hyperintense on the FLAIR-weighted MR image (**B**). In the periphery of the lesion, confluent hyperintense areas (arrowheads) are seen. Focal demyelinations (small arrows) are seen in the internal capsule and subependymal area adjacent to the frontal horn as well as in the parahippocampal gyrus and subependymal area adjacent to the trigone on the right side. FET-PET (**C**) co-registered with the T1-weighted MR image reveals high uptake of the lesion (arrow, SUV_{max} 6.0, TBR_{max} 5.2) and another small focus posteriorly (arrowhead).

Modern MS therapy is known to modulate the immune system in various and mainly suppressive ways. On the other hand, a functioning immune system is important for the response to tumors, and immunosuppression was shown to affect the prognosis in glioblastoma patients.[48,49]

We acknowledge several limitations of our study. First, we only included patients where the MR scan was equivocal, and can thus not comment on the diagnostic accuracy of MR vs. FET-PET imaging in a more general population of patients with demyelinating disease. The diagnostic accuracy of MR in our cohort is biased owing to these selective criteria, however, the diagnostic performance of MR was also not the thrust of our study. Notably, particularly patients with equivocal MR scans would be the cohort with potential benefits from FET-PET imaging, considering also the radiation burden from FET-PET. Second, FET-PET scans were acquired on different scanners. However, PET parameters such as SUV_{max} are a reproducible and standardized measure and all FET-PET procedures in our cohort followed an institutionally standardized protocol. For the TAC, we used 20–40 min. Other authors used various acquisition frames between 0 and 50 min for FET-PET studies, with 10–30 min being most commonly applied. In order to recognize basic radiotracer kinetic patterns as in our study, the 20–40 min and 10–30 min approaches are considered comparable. Recently, the dynamic 20–40 min acquisition has gained more attention.[36,50,51] Third, owing to the low number of subjects, we could not provide a subanalysis of separate TDD. However, the clinical and radiological presentation of different TDD is often similar. The sample size was rather small, although the inclusion period of our study covered more than a decade at a major tertiary care center. This is mainly owing to the infrequent nature of the analyzed pathology. Thus, future multicenter studies are desired. The small sample size might have affected the ROC calculation. Nevertheless, significantly different TBR_{max} and SUV_{max} between TDL and brain tumors were found. In addition, there is a lack of similar reports in the literature, which precludes a comparison of our results with data published by peers.

In conclusion, we found that FET-PET parameters TBR_{max} (cut-off 2.2) and SUV_{max} (cut-off 2.5) are able to distinguish tumefactive demyelinations from true neoplastic lesions. Our findings may offer benefits for patients with known or suspected demyelinating disease and equivocal MR imaging results with regard to tumefactive lesions. Further prospective studies should be conducted in a multi-center setting, owing to the comparably low incidence of tumefactive lesions in patients with demyelinating disease.

ACKNOWLEDGMENT

The authors are indebted to Roland Martin, MD, for his support.

REFERENCES

1. Lucchinetti CF, Gavrilova RH, Metz I, et al. Clinical and radiographic spectrum of pathologically confirmed tumefactive multiple sclerosis. *Brain*. 2008;131:1759–1775.
2. Lucchinetti C, Brück W, Parisi J, et al. Heterogeneity of multiple sclerosis lesions: implications for the pathogenesis of demyelination. *Ann Neurol*. 2000;47:707–717.
3. Given CA 2nd, Stevens BS, Lee C. The MRI appearance of tumefactive demyelinating lesions. *AJR Am J Roentgenol*. 2004;182:195–199.
4. Kepes JJ. Large focal tumor-like demyelinating lesions of the brain: intermediate entity between multiple sclerosis and acute disseminated encephalomyelitis? A study of 31 patients. *Ann Neurol*. 1993;33:18–27.
5. Malo-Pion C, Lambert R, Decarie JC, et al. Imaging of acquired demyelinating syndrome with 18F-FDG PET/CT. *Clin Nucl Med*. 2018;43:103–105.
6. Altintas A, Petek B, Isik N, et al. Clinical and radiological characteristics of tumefactive demyelinating lesions: follow-up study. *Mult Scler*. 2012;18:1448–1453.
7. Frederick MC, Cameron MH. Tumefactive demyelinating lesions in multiple sclerosis and associated disorders. *Curr Neurol Neurosci Rep*. 2016;16:26.
8. Patriarca L, Torlone S, Ferrari F, et al. Is size an essential criterion to define tumefactive plaque? MR features and clinical correlation in multiple sclerosis. *Neuroradiol J*. 2016;29:384–389.
9. Masdeu JC, Quinto C, Olivera C, et al. Open-ring imaging sign: highly specific for atypical brain demyelination. *Neurology*. 2000;54:1427–1433.
10. Poser S, Luer W, Bruhn H, et al. Acute demyelinating disease. Classification and non-invasive diagnosis. *Acta Neurol Scand*. 1992;86:579–585.
11. Paty DW, Oger JJ, Kastrukoff LF, et al. MRI in the diagnosis of MS: a prospective study with comparison of clinical evaluation, evoked potentials, oligoclonal banding, and CT. *Neurology*. 1988;38:180–185.
12. Torisu H, Kira R, Ishizaki Y, et al. Clinical study of childhood acute disseminated encephalomyelitis, multiple sclerosis, and acute transverse myelitis in Fukuoka Prefecture, Japan. *Brain Dev*. 2010;32:454–462.
13. Pohl D, Hennemuth I, von Kries R, et al. Paediatric multiple sclerosis and acute disseminated encephalomyelitis in Germany: results of a nationwide survey. *Eur J Pediatr*. 2007;166:405–412.
14. Chaodong Wang, Zhang KN, Wu XM, et al. Balo's disease showing benign clinical course and co-existence with multiple sclerosis-like lesions in Chinese. *Mult Scler*. 2008;14:418–424.
15. Dong A, Gao M, Wang Y, et al. FDG PET/CT in acute tumefactive multiple sclerosis occurring in a case of chronic graft-versus-host disease after allogeneic hematopoietic stem cell transplantation. *Clin Nucl Med*. 2016;41:e414–e416.
16. Golombievski EE, McCoyd MA, Lee JM, et al. Biopsy proven tumefactive multiple sclerosis with concomitant glioma: case report and review of the literature. *Front Neurol*. 2015;6:150.
17. Kebir S, Gaertner FC, Mueller M, et al. 18F-fluoroethyl-L-tyrosine positron emission tomography for the differential diagnosis of tumefactive multiple sclerosis versus glioma: a case report. *Oncol Lett*. 2016;11:2195–2198.
18. Preziosa P, Sangalli F, Esposito F, et al. Clinical deterioration due to co-occurrence of multiple sclerosis and glioblastoma: report of two cases. *Neurol Sci*. 2017;38:361–364.
19. Bahmanyar S, Montgomery SM, Hillert J, et al. Cancer risk among patients with multiple sclerosis and their parents. *Neurology*. 2009;72:1170–1177.
20. Anderson M, Hughes B, Jefferson M, et al. Gliomatous transformation and demyelinating diseases. *Brain*. 1980;103:603–622.
21. Sumelahti ML, Pukkala E, Hakama M. Cancer incidence in multiple sclerosis: a 35-year follow-up. *Neuroepidemiology*. 2004;23:224–227.
22. Plantone D, Renna R, Sbardella E, et al. Concurrence of multiple sclerosis and brain tumors. *Front Neurol*. 2015;6:40.
23. Rapp M, Heinzel A, Galldiks N, et al. Diagnostic performance of 18F-FET PET in newly diagnosed cerebral lesions suggestive of glioma. *J Nucl Med*. 2013;54:229–235.
24. Calcagni ML, Galli G, Giordano A, et al. Dynamic O-(2-[18F]fluoroethyl)-L-tyrosine (F-18 FET) PET for glioma grading: assessment of individual probability of malignancy. *Clin Nucl Med*. 2011;36:841–847.
25. Popperl G, Kreth FW, Mehrkens JH, et al. FET PET for the evaluation of untreated gliomas: correlation of FET uptake and uptake kinetics with tumour grading. *Eur J Nucl Med Mol Imaging*. 2007;34:1933–1942.
26. Bosnyak E, Michelhaugh SK, Klinger NV, et al. Prognostic molecular and imaging biomarkers in primary glioblastoma. *Clin Nucl Med*. 2017;42:341–347.
27. Wester HJ, Herz M, Weber W, et al. Synthesis and radiopharmacology of O-(2-[18F]fluoroethyl)-L-tyrosine for tumor imaging. *J Nucl Med*. 1999;40:205–212.
28. Weckesser M, Langen KJ, Rickert CH, et al. O-(2-[18F]fluorethyl)-L-tyrosine PET in the clinical evaluation of primary brain tumours. *Eur J Nucl Med Mol Imaging*. 2005;32:422–429.
29. Chan M, Hsiao E. Neurosarcoidosis on FET and FDG PET/CT. *Clin Nucl Med*. 2017;42:197–199.
30. Hutterer M, Bumes E, Riemenschneider MJ, et al. AIDS-related central nervous system toxoplasmosis with increased 18F-fluoroethyl-L-tyrosine amino acid PET uptake due to LAT1/2 expression of inflammatory cells. *Clin Nucl Med*. 2017;42:e506–e508.
31. Floeth FW, Pauleit D, Sabel M, et al. Prognostic value of O-(2-18F-fluoroethyl)-L-tyrosine PET and MRI in low-grade glioma. *J Nucl Med*. 2007;48:519–527.
32. Pöpperl G, Götz C, Rachinger W, et al. Value of O-(2-[18F]fluoroethyl)-L-tyrosine PET for the diagnosis of recurrent glioma. *Eur J Nucl Med Mol Imaging*. 2004;31:1464–1470.

33. Filss CP, Galldiks N, Stoffels G, et al. Comparison of 18F-FET PET and perfusion-weighted MR imaging: a PET/MR imaging hybrid study in patients with brain tumors. *J Nucl Med*. 2014;55:540–545.
34. Jena A, Taneja S, Gambhir A, et al. Glioma recurrence versus radiation necrosis: single-session multiparametric approach using simultaneous O-(2-18F-fluoroethyl)-L-tyrosine PET/MRI. *Clin Nucl Med*. 2016;41:e228–e236.
35. Dunet V, Rossier C, Buck A, et al. Performance of 18F-fluoro-ethyl-tyrosine (18F-FET) PET for the differential diagnosis of primary brain tumor: a systematic review and metaanalysis. *J Nucl Med*. 2012;53:207–214.
36. Ceccon G, Lohmann P, Stoffels G, et al. Dynamic O-(2-18F-fluoroethyl)-L-tyrosine positron emission tomography differentiates brain metastasis recurrence from radiation injury after radiotherapy. *Neuro Oncol*. 2017;19:281–288.
37. Annesley-Williams D, Farrell MA, Staunton H, et al. Acute demyelination, neuropathological diagnosis, and clinical evolution. *J Neuropathol Exp Neurol*. 2000;59:477–489.
38. Zagzag D, Miller DC, Kleinman GM, et al. Demyelinating disease versus tumor in surgical neuropathology. Clues to a correct pathological diagnosis. *Am J Surg Pathol*. 1993;17:537–545.
39. Kobayashi M, Shimizu Y, Shibata N, et al. Gadolinium enhancement patterns of tumefactive demyelinating lesions: correlations with brain biopsy findings and pathophysiology. *J Neurol*. 2014;261:1902–1910.
40. Gempt J, Soehngen E, Förster S, et al. Multimodal imaging in cerebral gliomas and its neuropathological correlation. *Eur J Radiol*. 2014;83:829–834.
41. Balashov KE, Aung LL, Dhib-Jalbut S, et al. Acute multiple sclerosis lesion: conversion of restricted diffusion due to vasogenic edema. *J Neuroimaging*. 2011;21:202–204.
42. Tievsky AL, Ptak T, Farkas J. Investigation of apparent diffusion coefficient and diffusion tensor anisotrophy in acute and chronic multiple sclerosis lesions. *AJNR Am J Neuroradiol*. 1999;20:1491–1499.
43. Castriota-Scanderbeg A, Sabatini U, Fasano F, et al. Diffusion of water in large demyelinating lesions: a follow-up study. *Neuroradiology*. 2002;44:764–767.
44. Dagher AP, Smirniotopoulos J. Tumefactive demyelinating lesions. *Neuroradiology*. 1996;38:560–565.
45. Peterson K, Rosenblum MK, Powers JM, et al. Effect of brain irradiation on demyelinating lesions. *Neurology*. 1993;43:2105–2112.
46. Dietrich J, Rao K, Pastorino S, et al. Corticosteroids in brain cancer patients: benefits and pitfalls. *Expert Rev Clin Pharmacol*. 2011;4:233–242.
47. McLean JS, Frame MC, Freshney RI, et al. Phenotypic modification of human glioma and non-small cell lung carcinoma by glucocorticoids and other agents. *Anticancer Res*. 1986;6:1101–1106.
48. Madkouri R, Kaderbhai CG, Bertaut A, et al. Immune classifications with cytotoxic CD8+ and Th17 infiltrates are predictors of clinical prognosis in glioblastoma. *Oncoimmunology*. 2017;6:e1321186.
49. Rühle PF, Goerig N, Wunderlich R, et al. Modulations in the peripheral immune system of glioblastoma patient is connected to therapy and tumor progression—a case report from the IMMO-GLIO-01 Trial. *Front Neurol*. 2017;8:296.
50. Tscherpel C, Dunkl V, Ceccon G, et al. The use of O-(2-18F-fluoroethyl)-L-tyrosine PET in the diagnosis of gliomas located in the brainstem and spinal cord. *Neuro Oncol*. 2017;19:710–718.
51. Albatly AA, Alsamarah AT, Alhawas A, et al. Value of ^{18}F-FET PET in adult brainstem glioma. *Clin Imaging*. 2018;51:68–75.